PNAS RESEARCH ARTICLE

Tianyang Mao[a,1], Jooyoung Kim[b,c,1], Mario A. Peña-Hernández[a,d,1], Gabrielee Valle[b], Miyu Moriyama[a], Sophia Luyten[a], Isabel M. Ott[a], Maria Luisa Gomez-Calvo[a], Jeff R Gehlhausen[e], Emily Baker[e], Benjamin Israelow[a,f], Martin Slade[g], Lokesh Sharma[b,c], Wei Liu[b], Changwan Ryu[b], Asawari Korde[b], Chris J. Lee[b], Valter Silva Monteiro[a], Carolina Lucas[a], Huiping Dong[a], Yi Yang[a], Yale SARS-CoV-2 Genomic Surveillance Initiative[2], Smita Gopinath[h], Craig B. Wilen[a,i], Noah Palm[a], Charles S. Dela Cruz[b,c,j,3], and Akiko Iwasaki[a,e,k,l,3]

Contributed by Akiko Iwasaki; received November 7, 2023; accepted March 15, 2024; reviewed by Cecilia Johannson and Ivan Zanoni

Respiratory virus infections in humans cause a broad-spectrum of diseases that result in substantial morbidity and mortality annually worldwide. To reduce the global burden of respiratory viral diseases, preventative and therapeutic interventions that are accessible and effective are urgently needed, especially in countries that are disproportionately

Significance

Respiratory virus infections in humans are a significant global health concern, causing a wide range of diseases with substantial morbidity and mortality worldwide. This underscores the urgent need for effective interventions to reduce the burden of respiratory viral diseases, especially in countries disproportionately affected. In this work, we repurpose a widely available generic medication, neomycin, as a host-directed antiviral strategy to combat upper respiratory viral infection and transmission, offering hope for addressing a significant global health challenge.

Author contributions: T.M., M.A.P.-H., S.G., C.S.D.C., and A.I. designed research; T.M., J.K., M.A.P.-H., G.V., M.M., S.L., I.M.O., M.L.G.-C., J.R.G., E.B., B.I., L.S., W.L., C.R., A.K., C.J.L., V.S.M., C.L., H.D., Y.Y., and Y.S.G.S.I. performed research; M.S., C.B.W., and N.P. contributed new reagents/analytic tools; T.M., J.K., M.A.P.-H., M.M., M.L.G.-C., and J.R.G. analyzed data; and T.M. and A.I. wrote the paper.

Reviewers: C.J., Imperial College London; and I.Z., Boston Children's Hospital.

Competing interest statement: A.I.

Intranasal Neomycin Treatment Induces an ISG Response in the Nasal Mucosa that Is Independent of Commensal Microbiota

Irf7, *Isg15*, *Usp18*, *Cxcl10*, *Rsad2*, *Cxcl10*

Neomycin-Triggered ISG Response Does Not Require Type I or III IFN Receptor Signaling

Single-Dose Intranasal Neomycin Prophylaxis Affords Antiviral Protection against SARS-CoV-2 Infection and Disease

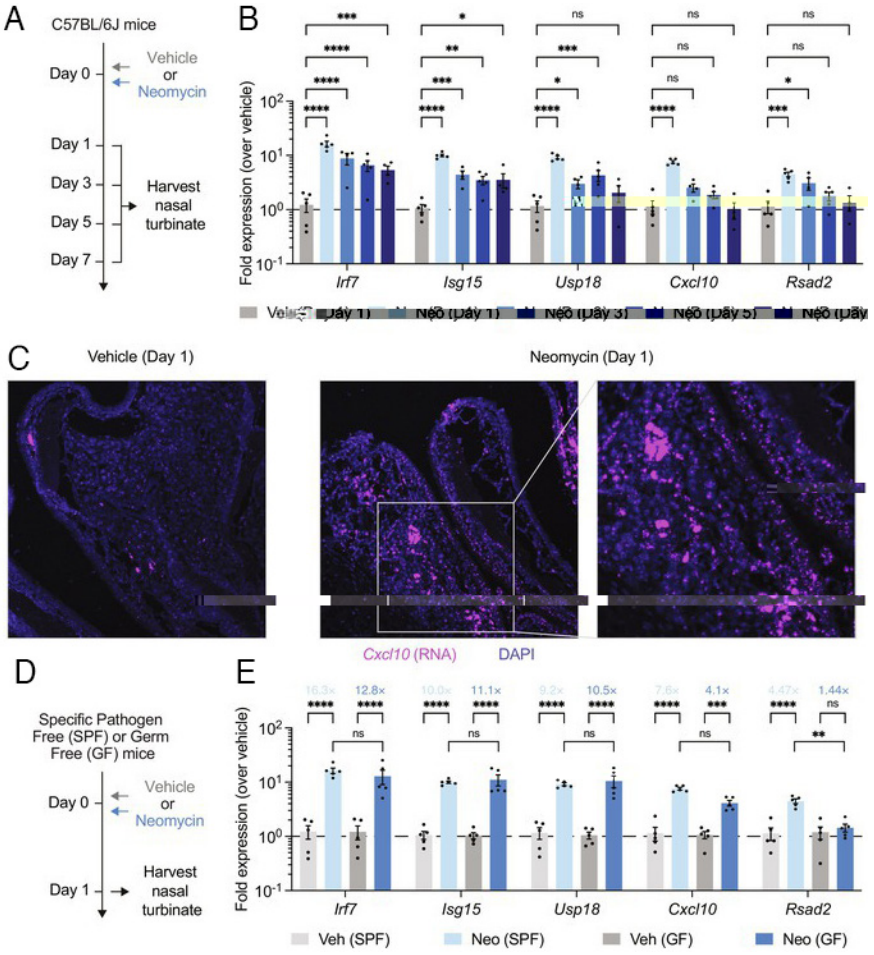

Fig. 1. Intranasal application of neomycin induces an upper respiratory ISG response independent of commensal microbiota. (*A*) Experimental schema. Specific-pathogen-free (SPF) C57BL/6J mice were intranasally treated once with 2 mg neomycin, or vehicle delivered in 10 μL volume per nostril. On days 1, 3, 5, and 7 posttreatment, nasal turbinates were collected for gene expression analysis by RT-qPCR and for RNA FISH analysis (for day 1 tissues only). (*B*) Expression of ISGs *Irf7*, *Isg15*, *Usp18*, *Cxcl10*, and *Rsad2* in nasal turbinate tissues (Day 1, n = 5; Day 3, n = 4; Day 5, n = 5; Day 7, n = 4). Gene expression was normalized against housekeeping genes *Hprt*, and then compared against biological controls (vehicle-treated mice). (*C*) RNA FISH analysis of *Cxcl10* expression in paraffin-embedded nasal turbinate tissues. (*D*) Experimental schema. SPF or GF mice were intranasally treated once with 2 mg neomycin or vehicle. On day 1 posttreatment, nasal turbinates were collected for gene expression analysis by RT-qPCR. (*E*) Expression of ISGs *Irf7*, *Isg15*, *Usp18*, *Cxcl10*, and *Rsad2* in nasal turbinate tissues (SPF + Vehicle, n = 5; SPF + Neomycin, n = 5; GF + Vehicle, n = 5; GF + Neomycin, n = 5). Gene expression of SPF and GF samples were separately compared to their vehicle controls. To reduce the overall number of experimental animals used, control data points from naïve and neomycin-treated animals housed in the SPF facility are common to *B* and *E*. For RNA FISH analyses, representative staining results were shown. Sections are representative of multiple sections from at least five mice per group. Mean ± SEM; statistical significance was calculated by means of two-way ANOVA followed by Tukey's correction (*B* and *E*); $*P \le 0.05$, $**P \le 0.01$, $***P \le 0.001$, $****P \le 0.0001$. Individual data points are represented. Samples from different timepoints were collected from different animals, not the same animals longitudinally.

(*B* *C*)

( )

(*D*) (*G* *I*)

( ) (*E*)

( )

(*F*)

( )

Intranasal Neomycin Treatment Confers Protection against Influenza A Virus Infection

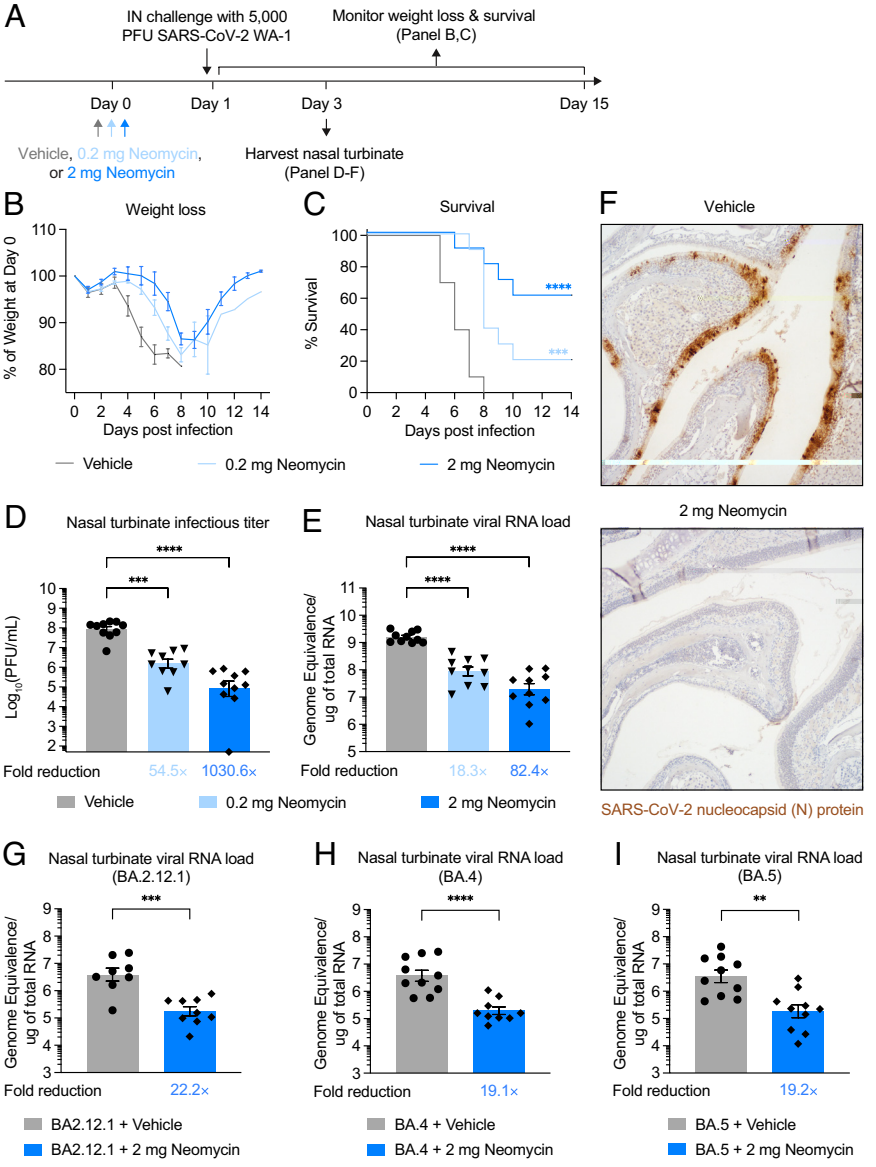

Fig. 2. Neomycin prophylaxis affords antiviral protection against SARS-CoV-2 infection and disease. (*A*) Experimental schema. K18-hACE2 mice housed in a SPF facility were intranasally treated once with 0.2 mg neomycin, 2 mg neomycin or vehicle delivered in 10 μL volume per nostril. One day after treatment, mice were intranasally infected with 5×10^3 PFU SARS-CoV-2 (2019n-CoV/USA_WA1/2020). In one group of mice, weight loss and survival were monitored daily up to 14 DPI. Death was recorded when mice were moribund, or at 80% of original body weight. In a separate cohort, nasal turbinate tissues were collected for viral titer analysis 2 DPI. (*B* and *C*) Weight loss and survival of K18-hACE2 mice prophylactically treated with vehicle, 0.2 mg neomycin, or 2 mg neomycin from 1 to 14 DPI (Vehicle, n = 10; 0.2 mg Neomycin, n = 10; 2 mg Neomycin, n = 10). (*D*) Measurement of infectious virus titer in the nasal turbinate at 2 DPI by plaque assay (Vehicle, n = 10; 0.2 mg Neomycin, n = 9; 2 mg Neomycin, n = 10). Limit of detection (LOD): 10^2 PFU/mL. (*E*) Measurement of vRNA in the nasal turbinate at 2 DPI by RT-qPCR against SARS-CoV-2 N gene using the CDCN1 primer-probe set (Vehicle, n = 10; 0.2 mg Neomycin, n = 10; 2 mg Neomycin, n = 10). (*F*) Representative images of immunohistochemistry staining of SARS-CoV-2 N protein on nasal turbinate sections from vehicle- or neomycin-treated mice. (*G–I*) Measurement of vRNA in the nasal turbinate at 2 DPI from mice infected with BA.2.12.1, BA.4 or BA.5 by RT-qPCR against SARS-CoV-2 N gene using the CDCN1 primer-probe set (BA2.12.1 + Vehicle, n = 8; BA2.12.1 + Neomycin, n = 9; BA.4 + Vehicle, n = 10; BA.4 + Neomycin, n = 9; BA.5 + Vehicle, n = 10; BA.5 + Neomycin, n = 10). Fold reduction was calculated as average fold reduction in infectious (*D*) or genomic RNA (*E* and *G–I*) virus load between neomycin-treated groups and vehicle controls. For histological analyses, representative H&E staining results were shown. Sections are representative of multiple sections from at least five mice per group. Mean ± SEM; statistical significance was calculated by the log-rank Mantel–Cox test (*C*), one-way ANOVA followed by Tukey correction (*D* and *E*) or Student's *t* test (*G–I*). Individual data points are represented. Data are pooled from two independent experiments.

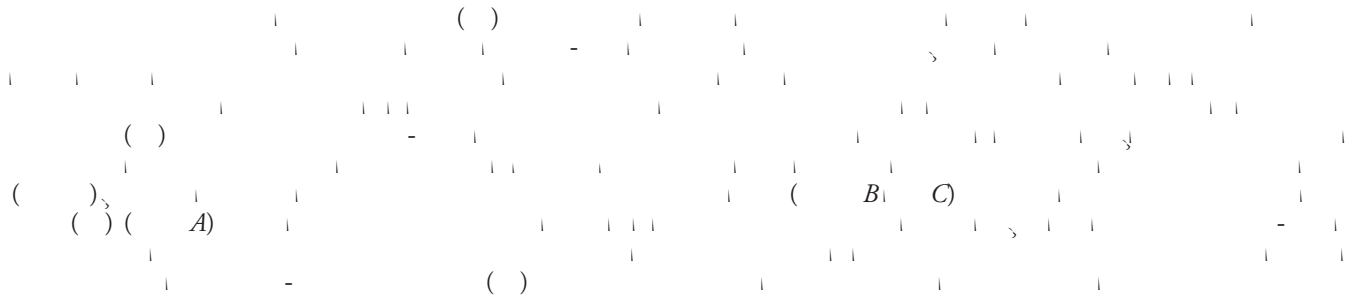

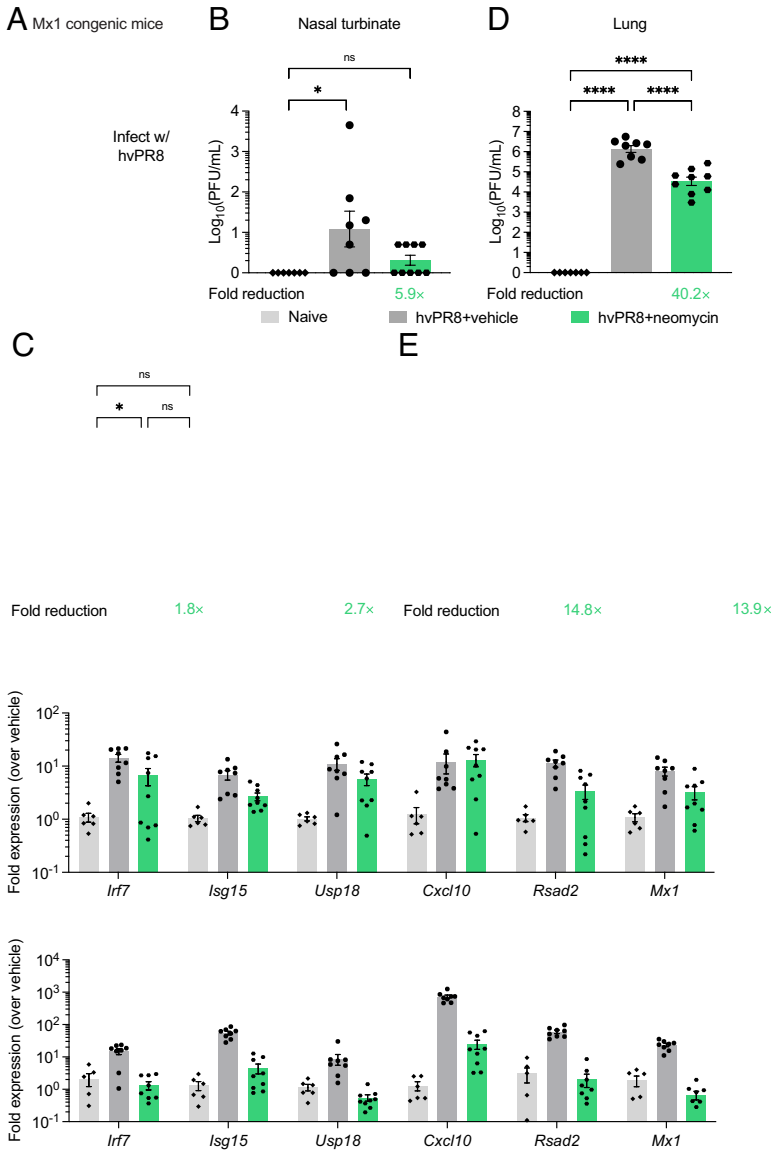

μ

Irf7, *Rsad2*, *Mx1*, *Isg15*, *Usp18*, (*D*, *E*) - (*G*) (*F*) -

Intranasal Neomycin Therapy Mitigates Disease and Curbs Infection of SARS-CoV-2

Intranasal Neomycin Reduces Transmission in a Hamster Model of COVID-19

Intranasal Neosporin Application Induces Variable ISG Induction in Healthy Humans

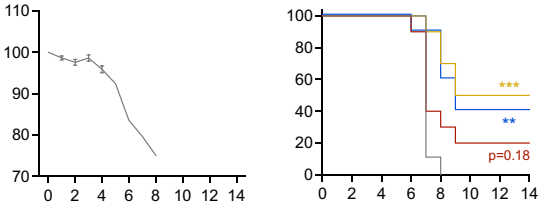
110
100
90
80
70
0 2 4 6 8 10 12 14
100
80
60
40
20
0
0 2 4 6 8 10 12 14
***
**
p=0.18

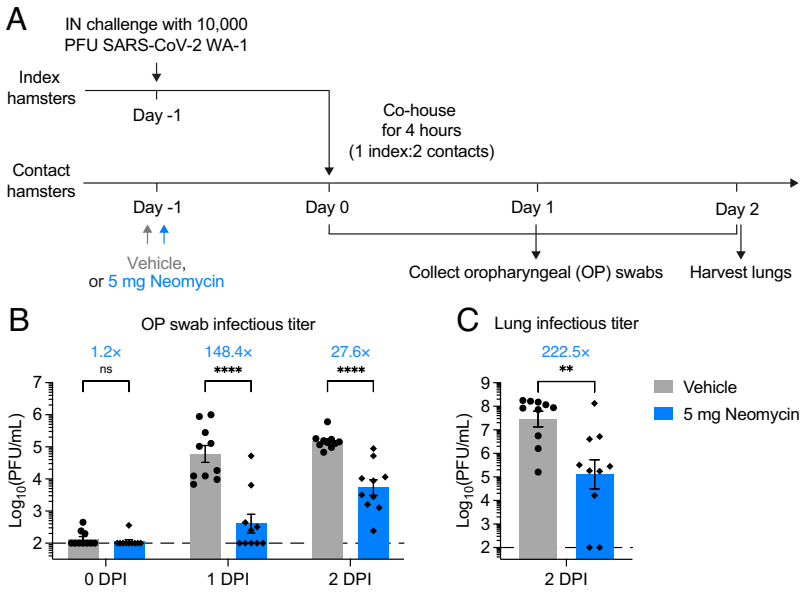

Fig. 5. Neomycin reduces contact transmission in a hamster model of SARS-CoV-2. (*A*) Transmission experimental schema. Syrian hamsters were intranasally treated with 5 mg of neomycin or vehicle delivered in 25 µL volume per nostril. Twenty-four hours after neomycin treatment, recipient hamsters were cohoused for 4 h with naïve donor hamsters that had been infected 24 h earlier with 10^4 PFU SCV2. Daily OP swabs from 0 to 2 DPI as well as lung tissues on 2 DPI were collected. (*B*) Measurement of infectious virus titer in OP swabs on 0 to 2 DPI by plaque assay (Vehicle, n = 10; Neomycin, n = 10). (*C*) Measurement of infectious virus titer in lung tissues on 2 DPI by plaque assay (Vehicle, n = 10; Neomycin, n = 10). Fold reduction was calculated as average fold reduction in infectious (*B* and *C*) virus load between neomycin-treated groups and vehicle controls and indicated above all bar plots. Mean ± SEM; statistical significance was calculated by means of one-way ANOVA followed by Tukey's correction (*B*) or Student's *t* test (*C*). *$P \le 0.05$, **$P \le 0.01$, ***$P \le 0.001$, ****$P \le 0.0001$. Individual data points are represented. Data are pooled from two independent experiments.

Ifnar
-β

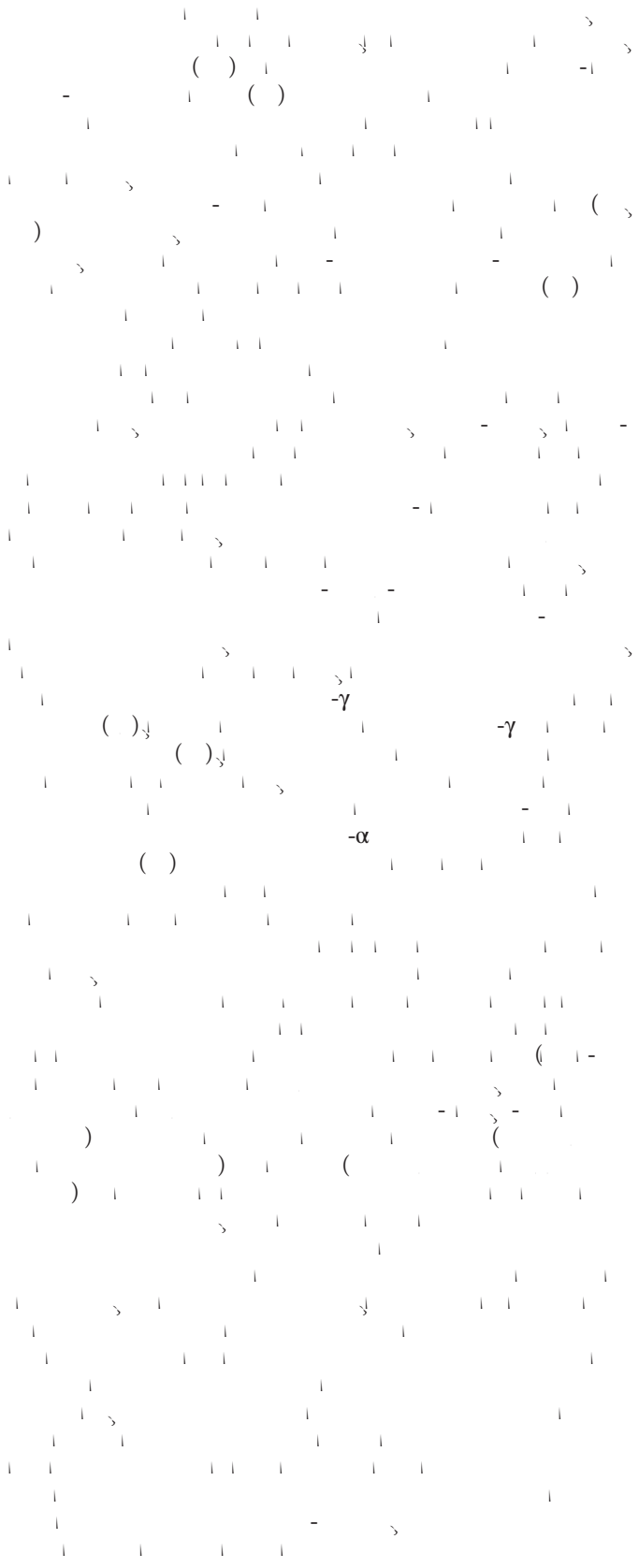

Materials and Methods

Animals. C57BL/6J (B6J) and B6.Cg-Tg(K18-ACE2)2Prlmn/J (K18-hACE2) mice were purchased from The Jackson Laboratory and subsequently bred and housed at Yale University. C57BL/6 mice carrying functional Mx1 alleles were a gift from P. Staeheli (University Medical Center Freiburg). Syrian hamsters (Strain HSdHan:AURA; stock no. 089) were purchased from Envigo. Animals were fed with regular rodent's chow and sterilized water ad libitum, and maintained on a 12-h light/dark cycle under SPF conditions. For GF experiments, C57BL/6 mice were maintained in flexible plastic gnotobiotic isolators with a 12-h light/dark cycle and provided with a standard, autoclaved mouse chow ad libitum and autoclaved water. GF status was monitored by culture-based and culture-independent methods. All procedures used in this study (sex-matched and age-matched) complied with federal guidelines and the institutional policies of the Yale School of Medicine Institutional Animal Care and Use Committee (IACUC), under protocol #10365.

Cells and Viruses. SARS-CoV-2 isolate hCOV-19/USA-WA1/2020 (NR-52281) was obtained from BEI Resources and was amplified in VeroE6 cells overexpressing ACE2 and TMPRSS2 (kindly provided by B. Graham at the NIH Vaccine Research Center), as previously described. Viral titers were determined with standard plaque assay by using Vero E6 cells overexpressing hACE2 and TMPRSS2. SARS-CoV-2 omicron variants were isolated from nasopharyngeal swabs of infected individuals. Samples belonging to the BA2.12.1, BA.4, and BA.5 lineages were selected for virus isolation as previously described. The highly virulent variant of A/PR8 was a gift from P. Staeheli (University Medical Center, Freiburg). Influenza virus strain A/PR/8/34 (H1N1) was propagated as previously described (43). Cell lines obtained from ATCC were not further authenticated and all cell lines were routinely tested for mycoplasma contamination.

Virus Infection. Before infection, mice were anesthetized using a mixture of ketamine and xylazine injected intraperitoneally. K18-hACE2 mice were intranasally infected with 5×10^3 PFU SARS-

Measurements of Influenza Genomic RNA and Infectious Virus. At indicated time points, mice were euthanized with 100% isoflurane. The whole lung or nasal turbinate was placed in a Lysing Matrix D tube (MP Biomedicals) with 1 mL PBS and homogenized using a table-top homogenizer at medium speed for 2 min. Tissue homogenates were cleared of debris by centrifugation (15 min, 3,100 g). To determine infectious influenza viral titers, plaque assay was performed by standard protocol using Madin-Darby canine kidney (MDCK) cells. Briefly, plaques were resolved by crystal violet staining 48 to 72 h after infection and rinsing with water for plaque visualization. For viral RNA analysis, 250 μL of the nasal turbinate or lung homogenates was added to 750 μL Trizol LS (Invitrogen), and RNA was extracted with the RNeasy Mini Kit (Qiagen) according to the manufacturer's instructions. The extracted RNA was reverse transcribed into cDNA using the iScript cDNA synthesis kit (Bio-Rad). Influenza A/PR8 RNA levels were quantified with 100 ng cDNA inputs using the iTaq Universal SYBR Green Supermix (Bio-Rad) and the following primers (5′–3′): PR8 hemagglutinin (Forward: AGTGCCCAAAATACGTCAGG, Reverse: GGCAATGGCTCCAAATAGAC), PR8 nucleoprotein (Forward: AGAACATCTGACATGAGGAC, Reverse: GTCAAAGGAAGGCACGATC).

Measurements of Mouse Gene Expression by RT-qPCR. Following RNA extraction, total cDNA was prepared with 2 μg RNA inputs using the iScript cDNA Synthesis Kit following the manufacturer's instruction (Bio-Rad). RT-qPCR was then performed using the SYBR Green PCR Master Mix (Applied Biosystems). For each RT-qPCR, 100 ng cDNA input was used. The following primers were used for mouse ISG expression *H* (Forward: TCAGTCAACGGGGGACATAAA, Reverse: GGGGCTGTACTGCTTAACCAG); *I 15* (Forward: GCTAGAGCCTGCAGCAATG, Reverse: CCAATCTTCTGGGCAATCTGC); *I 7* (Forward: TGTAGACGGAGCAATGGCTGAAGT, Reverse: ATCCCTACGACCGAAATGCTTCCA); *U 18* (Forward: CGTGCTTGAGAGGGTCATTTG, Reverse: GGTCCGGAGTCCACAACTTC); *C 10* (Forward: AGAATGAGGGCCATAGGGAA, Reverse: CGTGGCAATGATCTCAACAC); *R 2* (Forward: AACAGGCTGGTTTGGAGAAG, Reverse: TGCCATTGCTCACTATGCTC); *M 1* (Forward: GACCATAGGGGTCTTGACCAA, Reverse: (AGACTTGCTCTTTCTGAAAAGCC). RT-qPCRs were run in duplicates. The duplicate Ct values were averaged, normalized against housekeeping genes *H* (for mouse) or *GAPDH* (for human), and then compared against biological controls (untreated mice) using the ΔΔCt method of comparison. Fold expression was calculated assuming a doubling efficiency (2) per cycle (fold expression = $2^{-\Delta\Delta Ct}$).

Immunohistochemistry. The head was fixed in a 4% paraformaldehyde buffer overnight at 4 °C, then transferred into 1 M ethylenediaminetetraacetic acid (EDTA) solution (Invitrogen) at pH 8.0 for 7 d at 4 °C, changing the EDTA solution once on day 4. After decalcification, Yale Pathology Tissue Services (YPTS) performed formalin fixed paraffin embedding, sectioning, and immunohistochemical staining of nasal tissues. For SARS-CoV-2 N protein staining, polyclonal rabbit-derived IgG (GeneTex; GTX135357) were used at recommended dilutions. Stained sections were then imaged by a fluorescence microscope (BX51; Olympus) with a 10× lens.

RNA FISH. RNA ISH was performed using the RNAScope kit (Bio-Techne, Cat # 323100) following the manufacturer's instructions. Decalcified tissues were embedded in paraffin and sliced into coronal cross-sections using a microtome. Slices were mounted on a glass slide. Slides were first deparaffinized, treated with hydrogen peroxide blocking step, and then with protease prior to using the RNAScope target antigen retrieval. Probe hybridization and amplification steps were followed per manufacturer protocol. Slides were stained with DAPI to visualize nuclei and mounted on slides using ProLong Gold Antifade (ThermoFisher, Cat # P36934). The *C 10* probe was purchased from Bio-Techne (Cat # 408921). Opal 690 Reagent (Akoya Biosciences, Cat # FP1497001KT) was used to visualize staining using a Stellaris 8 confocal microscope (Leica).

Determination of Determination of IFN-I, IFN-II, IFN-III, and IL-1α Concentration in Nasal Washes. Mice were euthanized with 100% isoflurane following the IACUC protocol #10365. After euthanasia, the head was removed from the mouse body, and the lower mandible was discarded from the snout. Nasal wash was performed by pushing 500 μL of PBS using a plastic tube attached to a 26-gauge needle through the nasopharynx into a 1.5 mL Eppendorf tube. Nasal washes were repeated 3 times. Samples were centrifuged at 3,900 rpm for 5 min at 4 °C; the supernatant was aliquoted in 100 μL aliquots and stored at −80 °C. Concentration of IFN-I in nasal washes was determined by ELISA (42120 and 42400; PBL Assay Science) as previously described. Concentration of IFN-λ in nasal washes was determined by ELISA (DY1789B; R&D Systems) as previously described. Concentration of IFN-γ in nasal washes was determined by ELISA (KMC4021; Invitrogen) according to the manufacturer's instructions. Concentration of IL-1α in nasal washes was determined by ELISA (BMS611; Invitrogen) according to the manufacturer's instructions.

Graphical Illustrations. Graphical illustrations were made with Biorender.com.

Data, Materials, and Software Availability. All study data are included in the article and/or supporting information.

ACKNOWLEDGMENTS. This work was supported by the Bill & Melinda Gates Foundation. A.I. is an investigator of the Howard Hughes Medical Institute. We thank J. Arm, C. Karp, and G. Means (Bill & Melinda Gates Foundation, Seattle, WA) for helpful feedback on the project. We thank M. Linehan for her logistical assistance. We thank B. Graham (NIH Vaccine Research Center, Bethesda, MD) for kindly providing VeroE6 cells overexpressing ACE2 and TMPRSS2. We thank P. Staeheli (Institute of Virology, Medical Center University of Freiburg, Freiburg, Germany) for kindly providing Mx1 congenic mice. We thank YPTS for their assistance with tissue embedding, sectioning, and immunohistochemistry staining. We thank the research staff members of Yale Center for Clinical Investigation (YCCI) who provided assistance in implementing the human studies protocol. We also give special recognition of the services of B. Fontes and the Yale Environmental Health and Safety Department for their continuing assistance in safely conducting biosafety level 3 research.

Author affiliations: [a]Department of Immunobiology, Yale University School of Medicine, New Haven, CT 06510; [b]Department of Internal Medicine, Section of Pulmonary, Critical Care and Sleep Medicine, Yale University School of Medicine, New Haven, CT 06510; [c]Division of Pulmonary, Allergy, Critical Care, and Sleep Medicine, Department of Medicine, University of Pittsburgh, Pittsburgh PA 15213; [d]Department of Microbial Pathogenesis, Yale University School of Medicine, New Haven CT 06510; [e]Department of Dermatology, Yale University School of Medicine, New Haven, CT 06510; [f]Department of Internal Medicine, Section of Infectious Diseases, Yale University School of Medicine, New Haven, CT 06510; [g]Department of Internal Medicine, Section of Occupational Medicine, Yale University School of Medicine, New Haven, CT 06510; [h]Department of Immunology and Infectious Diseases, Harvard T.H. Chan School of Public Health, Harvard University, Boston, MA 02115; [i]Department of Laboratory Medicine, Yale University School of Medicine, New Haven, CT 06510; [j]Veterans Affairs Pittsburgh Healthcare System, Pittsburgh, PA 15240; [k]Center for Infection and Immunity, Yale University School of Medicine, New Haven, CT 06510; and [l]HHMI, Chevy Chase, MD 20815

1. G. B. D. C. o. D. Collaborators, Global, regional, and national age-sex-specific mortality for 282 causes of death in 195 countries and territories, 1980–2017: A systematic analysis for the Global Burden of Disease Study 2017. *L* **392**, 1736–1788 (2018).
2. GBD 2017 Disease and Injury Incidence and Prevalence Collaborators, Global, regional, and national incidence, prevalence, and years lived with disability for 354 diseases and injuries for 195 countries and territories, 1990–2017: A systematic analysis for the Global Burden of Disease Study 2017. *L* **392**, 1789–1858 (2018).
3. N. H. L. Leung, Transmissibility and transmission of respiratory viruses. *N . R . M* . **19**, 528–545 (2021).
4. K. Tao ., SARS-CoV-2 antiviral therapy. *C . M . R* . **34**, e0010921 (2021).
5. N. Murakami ., Therapeutic advances in COVID-19. *N . R . N* . **19**, 38–52 (2023).
6. O. Demaria ., Harnessing innate immunity in cancer therapy. *N* **574**, 45–56 (2019).
7. W. M. Schneider, M. D. Chevillotte, C. M. Rice, Interferon-stimulated genes: A complex web of host defenses. *A . R* . **32**, 513–545 (2014).
8. E. Meffre, A. Iwasaki, Interferon deficiency can lead to severe COVID. *N* **587**, 374–376 (2020).
9. P. Bastard ., Autoantibodies against type I IFNs in patients with life-threatening COVID-19. *S* **370**, eabd4585 (2020).
10. Q. Zhang ., Inborn errors of type I IFN immunity in patients with life-threatening COVID-19. *S* **370**, eabd4570 (2020).
11. S. Gopinath ., Topical application of aminoglycoside antibiotics enhances host resistance to viral infections in a microbiota-independent manner. *N . M* . **3**, 611–621 (2018).
12. J. Klinkhammer ., IFN-lambda prevents influenza virus spread from the upper airways to the lungs and limits virus transmission. *E* **7**, e33354 (2018).
13. M. H. Orzalli ., An antiviral branch of the IL-1 signaling pathway restricts immune-evasive virus replication. *M . C* **71**, 825–840.e6 (2018).
14. P. B. McCray Jr. ., Lethal infection of K18-hACE2 mice infected with severe acute respiratory syndrome coronavirus. *J. V* . **81**, 813–821 (2007).
15. E. S. Winkler ., SARS-CoV-2 infection of human ACE2-transgenic mice causes severe lung inflammation and impaired function. *N* . **21**, 1327–1335 (2020).
16. S. F. Sia ., Pathogenesis and transmission of SARS-CoV-2 in golden hamsters. *N* **583**, 834–838 (2020).

17. M. Imai ., Syrian hamsters as a small animal model for SARS-CoV-2 infection and countermeasure development. *P . N . A . S . U.S.A.* **117**, 16587–16595 (2020).
18. P. F. Dos Santos ., ISG15-induced IL-10 is a novel anti-inflammatory myeloid axis disrupted during active tuberculosis. . **200**, 1434–1442 (2018).
19. A. von Delft ., Accelerating antiviral drug discovery: Lessons from COVID-19. *N . R . D D* . **22**, 585–603 (2023), 10.1038/s41573-023-00692-8.
20. E. C. Holmes ., Understanding the impact of resistance to influenza antivirals. *C . M . R* . **34**, e00224-20 (2021).
21. S. Gandhi ., De novo emergence of a remdesivir resistance mutation during treatment of persistent SARS-CoV-2 infection in an immunocompromised patient: A case report. *N . .* **13**, 1547 (2022).
22. R. S. Wallis, A. O'Garra, A. Sher, A. Wack, Host-directed immunotherapy of viral and bacterial infections: Past, present and future. *N . R* . **23**, 121–133 (2023).
23. T. Mao ., A stem-loop RNA RIG-I agonist protects against acute and chronic SARS-CoV-2 infection in mice. *J. E . M* . **219**, e20211818 (2021).
24. F. Humphries ., A diamidobenzimidazole STING agonist protects against SARS-CoV-2 infection. *S* . **6**, eabi9002 (2021).
25. D. A. Hoagland ., Leveraging the antiviral type I interferon system as a first line of defense against SARS-CoV-2 pathogenicity . **54**, 557–570.e5 (2021).
26. D. Jhuti ., Interferon treatments for SARS-CoV-2: Challenges and opportunities. *I . D . T* . **11**, 953–972 (2022).
27. P. D. Monk ., Safety and efficacy of inhaled nebulised interferon beta-1a (SNG001) for treatment of SARS-CoV-2 infection: A randomised, double-blind, placebo-controlled, phase 2 trial. *L R . M* . **9**, 196–206 (2021).
28. G. Reis ., Early treatment with pegylated interferon lambda for Covid-19. *N. E . J. M* . **388**, 518–528 (2023).
29. S. Marx ., RIG-I-induced innate antiviral immunity protects mice from lethal SARS-CoV-2 infection. *M . T . N A* **27**, 1225–1234 (2022).
30. M. W. Fried, Side effects of therapy of hepatitis C and their management. *H* **36**, S237–S244 (2002).
31. H. A. Nguyen ., The direct-medical costs associated with interferon-based treatment for Hepatitis C in Vietnam. *W O R* . **4**, 129 (2019).
32. F. M. Barros, H. Cheinquer, C. T. Tsuchiya, E. A. Santos, Cost-effectiveness analysis of treatment with peginterferon-alfa-2a versus peginterferon-alfa-2b for patients with chronic hepatitis C under the public payer perspective in Brazil. *C E . R . A* . **11**, 25 (2013).
33. G. Giovannoni, F. E. Munschauer III, F. Deisenhammer, Neutralising antibodies to interferon beta during the treatment of multiple sclerosis. *J. N . N . P* **73**, 465–469 (2002).
34. F. Matsuda ., Anti-interferon-alpha neutralizing antibody is associated with nonresponse to pegylated interferon-alpha plus ribavirin in chronic hepatitis C. *J. V H* . **19**, 694–703 (2012).
35. S. Grassin-Delyle ., Intranasal drug delivery: An efficient and non-invasive route for systemic administration: Focus on opioids. *P . T* . **134**, 366–379 (2012).
36. S. Hong ., Evidence that antibiotics bind to human mitochondrial ribosomal RNA has implications for aminoglycoside toxicity. *J. B . C* . **290**, 19273–19286 (2015).
37. E. J. Begg, M. L. Barclay, Aminoglycosides–50 years on. *B . J. C . P* . **39**, 597–603 (1995).
38. S. K. Moestrup ., Evidence that epithelial glycoprotein 330/megalin mediates uptake of polybasic drugs. *J. C . I* . **96**, 1404–1413 (1995).
39. T. Iyoda ., The CD8+ dendritic cell subset selectively endocytoses dying cells in culture and in vivo. *J. E . M* . **195**, 1289–1302 (2002).
40. M. Zhong, Y. Kadota, Y. Shimizu, E. Gohda, Induction of cytolytic activity and interferon-gamma production in murine natural killer cells by polymyxins B and E. *I* . **8**, 508–513 (2008).
41. M. Tamura, Y. Nagano, Modulation by polymyxin-B of the effects of interferon on human myelogenous leukemia-cells. *M* . **38**, 407–411 (1994).
42. J. D. Marshall ., Polymyxin B enhances ISS-mediated immune responses across multiple species. *C* . **229**, 93–105 (2004).
43. M. Moriyama, H. Takeyama, H. Hasegawa, T. Ichinohe, Induction of lung CD8(+) T cell responses by consecutive inoculations of a poly(I:C) influenza vaccine. *V* **35**, 6620–6626 (2017).
44. T. Mao ., Unadjuvanted intranasal spike vaccine elicits protective mucosal immunity against sarbecoviruses. *S* **378**, eabo2523 (2022).